Experimental validation of extended NO and Soot model for advanced HD Diesel Engine Combustion

2009-01-0683

Experimental Validation of Extended NO and Soot Model for Advanced HD Diesel Engine Combustion

X.L.J. Seykens, R.S.G. Baert, L.M.T. Somers
Eindhoven University of Technology

F.P.T. Willems
TNO Automotive

ABSTRACT

A computationally efficient engine model is developed based on an extended NO emission model and state-of-the-art soot model. The model predicts exhaust NO and soot emission for both conventional and advanced, high-EGR (up to 50 %), heavy-duty DI diesel combustion. Modeling activities have aimed at limiting the computational effort while maintaining a sound physical/chemical basis. The main inputs to the model are the fuel injection rate profile, in-cylinder pressure data and trapped in-cylinder conditions together with basic fuel spray information. Obtaining accurate values for these inputs is part of the model validation process which is thoroughly described. Modeling results are compared with single-cylinder as well as multi-cylinder heavy-duty diesel engine data. NO and soot level predictions show good agreement with measurement data for conventional and high-EGR combustion with conventional timing.

INTRODUCTION

The freedom to vary diesel engine settings for a given load and speed requirement has significantly increased over the last decades. This flexibility comes at the cost of a increased complexity of the engine control system annex algorithms. Real-time combustion models that predict heat release rate and emissions would be powerful and valuable tools for controller design, testing and calibration and thus reducing controller development time and costs. Moreover, such models could also be used as combustion state estimators in model based control strategies.

Preferably, a model should be based on actual physics and chemistry, i.e. phenomenological. This will result in a more generic model. However, to limit computational effort, previous attempts at such models mentioned in literature often had an empirical or semi-empirical character and needed an extensive and expensive set of data for fitting/training of the model, [1],[2],[3].

In the present paper, phenomenological models for both NO and soot formation will be briefly introduced. For more detailed information about the models the reader is referred [4]. The models are developed for both conventional high temperature combustion and for high-EGR low temperature combustion. The models are aimed as an extension to TNO's current mean value engine model library DYNAMO. Focus is on the model validation process and its results. The main steps taken during the validation process are thoroughly described. Modeling results are compared with NO exhaust gas concentrations and soot mass for both a single-cylinder and a multi-cylinder engine.

NO FORMATION MODEL

The present NO formation model was presented more thoroughly in [4]. This section contains a summary of the model. NO formation is only considered for the diffusive combustion phase. With conventional heavy-duty diesel combustion – usually – the majority of the fuel is burned in the diffusion controlled combustion phase.

The Engineering Meetings Board has approved this paper for publication. It has successfully completed SAE's peer review process under the supervision of the session organizer. This process requires a minimum of three (3) reviews by industry experts.

ISSN 0148-7191

SAE Customer Service: Tel: 877-606-7323 (inside USA and Canada)
Tel: 724-776-4970 (outside USA)
Fax: 724-776-0790
Email: CustomerService@sae.org
SAE Web Address: http://www.sae.org

Printed in USA

Furthermore, the equivalence ratio of the premixed burnt mixture is typically too fuel rich for significant NO formation, as experimentally confirmed by Dec [6]. Similarly, local in-cylinder Laser-Induced Fluorescence (LIF) measurements by Verbiezen et al. [7] showed very little NO formation up to the occurrence of the diffusion flame. The NO model follows the approach suggested by Murayama et al. [5] over thirty years ago, but with some differences as listed in [4]. In the used approach the amount of fuel that is burnt at a given crank angle value (within a step of 1 degree crank angle) is determined from a heat release rate analysis. The NO formation rate within the resulting package of combustion products is – at any instant – determined by the combined effect of the evolution of in-cylinder pressure and fresh oxidizer entrainment on package temperature and composition. The success of such approach depends on two important aspects: package initialization and package evolution. The most important characteristics of both aspects are summarized below:

Package initialization

FUEL MASS – The mass of fuel assigned to a new package is derived from a measured heat release rate profile.

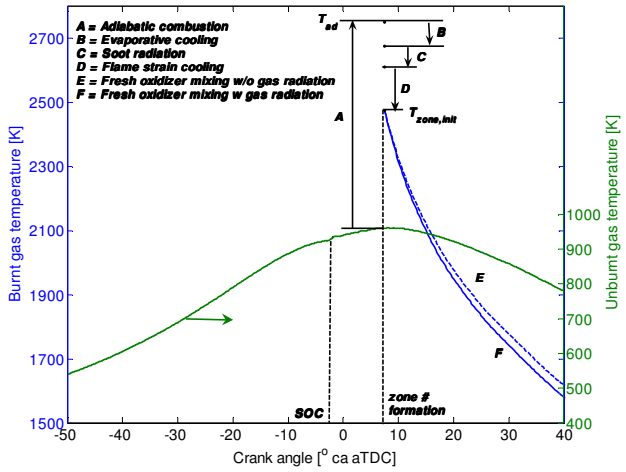

Figure 1 Graphical overview of initial combustion package temperature computation and subsequent evolution. Temperature corrections shown are qualitative; they are not representative for actual values.

INITIAL STATE – Initial combustion product temperature is based on the adiabatic flame temperature, including the effect of dissociation, computed using a chemical equilibrium solver based on minimizing Gibbs free energy. This temperature is corrected for the occurrence of several phenomena, as is graphically shown in Figure 1:

- *Evaporative cooling*: fuel evaporation extracts heat from the surroundings. By including the latent heat of evaporation into the computation of the adiabatic flame temperature, the flame temperature is corrected for this.
- *Hot soot particles radiative cooling:* Part of the wall heat transfer results from soot radiation. The radiative energy transferred during the crank angle of zone formation is used to correct the flame temperature.
- *Turbulence*: Turbulence results in so-called flame straining. At high levels of turbulence, physical time scales associated with the flow influence the chemical time scales. Equilibrium species concentration values are not reached which results in lower flame temperatures. One-dimensional diffusion flame computations with detailed chemistry have been used to quantify this temperature decrease. The inclusion of the influence of flame strain on NO formation is an extension to the model presented in [4].

Package evolution

After package formation, the combustion products are entrained with fresh oxidizer. It is well known that in modern DI diesel engines the fuel injection is the primary energy source driving the mixing process. In this study the mixing process is therefore linked to the fuel injection process: it is assumed that mixing of oxidizer into the combustion product packages is analogous to mixing of oxidizer into the fuel spray.

AIR ENTRAINMENT – The mixing process is described on the basis of the one-dimensional model for a free, fully developed, quasi-steady fuel spray as presented by Naber and Siebers [8]. This model gives the cross-sectional averaged equivalence ratio as a function of axial position along the spray axis:

$$\phi\left(\tilde{x}\right) = \frac{AFR_{st}}{\dot{m}_{ox}\left(\tilde{x}\right)/\dot{m}_f} = \frac{2 \cdot AFR_{st}}{\sqrt{1+16 \cdot \tilde{x}^2}-1} \qquad (1)$$

where AFR_{st} is the stoichiometric "air"-fuel ratio and $\tilde{x}$ is the normalized axial position in the spray. According to Siebers [9] the oxidizer entrainment into a diesel spray follows the relation:

$$\dot{m}_{ox}(x) \propto \sqrt{\rho_{ox} \cdot \rho_f} \cdot d_f \cdot x \cdot U_f \cdot \tan\left[\theta_{spray}/2\right] \qquad (2)$$

where ρ_{ox} and ρ_f are respectively the ambient oxidizer and fuel density, d_f is the diameter of the fuel stream at the injector nozzle hole exit, x is the axial position along the spray axis, U_f is the fuel exit velocity at the nozzle hole and θ_{spray} is the fuel spray cone angle.

As mentioned before, combustion products are assumed to be formed at the stoichiometric location. The model assumes that the equivalence ratio of a package continues to follow the relation described by equation (1) from this point onwards. In Figure 2 a graphical representation of this process is shown. Through this, every package is given a spatial position and can therefore also be referred to as a zone. The resulting temperature in the zones follows from solving the energy conservation equation.

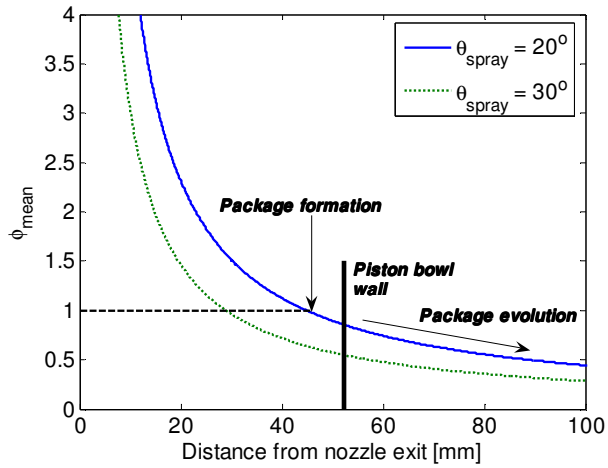

Figure 2 Evolution of 1-D quasi-steady spray according to model assumptions. $\bar{\rho}_{ox}$ = 30 kg/m^3, d_{noz} = 0.178 mm. Conditions as given in Table 2 for sweep D (14.0 bar IMEP at 1500 rpm) and SOA of -10 °ca aTDC.

TEMPERATURE CORRECTION – Hot species of CO, CO_2 and H_2O radiate to the environment. This results in a cooling of the hot combustion gases as is also graphically shown in Figure 1.

NO-FORMATION – The NO formation is computed as a post processing on the derived zone conditions. At any instant the species relevant for NO formation in a zone are assumed to be in chemical equilibrium as computed by the equilibrium solver. NO formation is computed according to the extended Zeldovich mechanism [10]. It is well-known that this mechanism can only account for NO formation at high temperatures (> 1800 K) [10]. In an attempt to capture NO formation for low temperature combustion, e.g. when high levels of EGR are applied, the main NO formation reaction of the N_2O-intermediate route is added:

$$N_2O + O \Leftrightarrow 2NO \qquad (3)$$

SOOT FORMATION MODEL

The soot formation model is strongly based on the zero dimensional soot model presented by Bayer and Foster [11]. Here, only a short summary of the model will be presented.

The soot model of Bayer and Foster is chosen because it describes soot formation in a burning diesel spray that follows the current conceptual view of diesel spray combustion as presented by Dec [12]. Besides this, through the used zero-dimensional approach, the model is also computationally efficient. This makes the model very suitable as a simulation tool in the controller development process.

The soot model is of the so-called two-step type as first suggested by Hiroyasu and Kadota [13]. The net soot production rate is the net effect of a soot formation and a soot oxidation contribution:

$$\frac{dm_s}{dt} = \frac{dm_{s,f}}{dt} - \frac{dm_{s,ox}}{dt} \qquad (4)$$

Commonly, this two-step mechanism is applied in a multi-dimensional environment, where soot production is computed for local conditions. Bayer and Foster have applied the mechanism on a macroscopic level. The soot formation and oxidation rates are computed for characteristic regions of temperature and equivalence ratio of the burning fuel spray.

Figure 3 shows a schematic and simplified representation of a lifted, steady, burning fuel spray. The injected fuel is vaporized by the entrainment of hot oxidizer. Initial fuel pyrolysis occurs at the rich initial premix reaction zone present just downstream of the liquid length LL. The spray interior is fed with the fuel-rich products of this initial reaction. In this region, conditions are ideal for soot formation: temperatures are high and oxygen concentration is low. In the spray interior, soot particles are formed which grow as they are transported through the spray. Finally, the particles are oxidized in the vicinity of the diffusion flame formed around the periphery of the spray plume where the soot particles are exposed to high temperatures and oxygen.

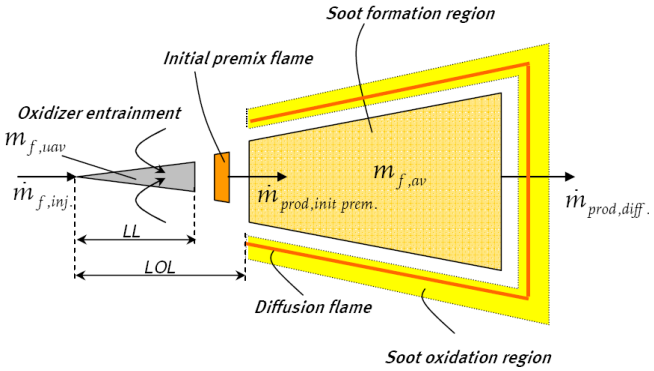

Figure 3 Schematic representation of a burning fuel spray with main regions of soot production process.

SOOT FORMATION – Following Bayer and Foster, the soot formation rate in equation (4) is given by the following expression:

$$\frac{dm_{s,f}}{dt} = C_{s,f} \cdot \bar{\phi}_{prem} \cdot m_{f,av} \cdot p^{0.5} \cdot e^{-\frac{E_{s,f}}{RT_{s,f}}} \qquad (5)$$

The pre-exponential factors include a soot-formation constant $C_{s,f}$, the mean equivalence ratio of the rich initial reaction $\bar{\phi}_{prem}$, the available fuel mass for soot formation $m_{f,av}$ and the pressure p. The soot formation constant is used to tune the model to a specific fuel type and engine. The soot formation temperature $T_{s,f}$ is equal to the combustion product temperature of the rich initial reaction at the equivalence ratio $\bar{\phi}_{prem}$. The temperature is computed using the chemical equilibrium solver. The

fuel mass available for soot formation follows from a mass balance between the injected fuel and the already burned fuel following from the rate of heat release.

In contrast to the soot formation equation of Hiroyasu and Kadota [13], equation (5) includes the mean equivalence ratio of the rich initial reaction $\bar{\phi}_{prem}$. This equivalence ratio is included by Bayer and Foster following the observations of Chomiak et al. [14]. They observed that the absolute mass of soot formed during a combustion cycle is linearly dependent on the equivalence ratio of the initial combustion. The probability of the available mass of fuel to actually transform into soot increases when $\bar{\phi}_{prem}$ is increased. Values of $\bar{\phi}_{prem}$ are typically in the range of 2 – 7 [14],[15].

Oxidizer can only be entrained into that part of the spray not sheathed by the diffusion flame. As a result, the equivalence ratio of the initial reaction is dependent on the so-called flame lift-off length *LOL,* see Figure 3: the distance between the nozzle and the most upstream location of combustion as found by Siebers and Higgins [15]. The *LOL* is determined using a semi-empirical correlation [11]. The equivalence ratio of the rich initial reaction is taken equal to the spray cross sectional averaged equivalence at the position of the *LOL* as follows from the one-dimensional spray model, see equation (1).

SOOT OXIDATION – Soot oxidation is assumed to occur in the vicinity of the stoichiometric diffusion flame. The soot oxidation rate is again given by an Arrhenius-type expression:

$$\frac{dm_{s,ox}}{dt} = C_{ox} \cdot m_s \cdot X_{O_2,st}^{C_{O_2}} \cdot p^{1.8} \, e^{-\frac{E_{s,ox}}{RT_{s,ox}}} \qquad (6)$$

The pre-exponential factors include a tuning constant $C_{s,ox}$, the mass of soot m_s, the molar fraction of oxygen at the stoichiometric diffusion flame $X_{O_2,st}$ and the pressure p. The exponent C_{O_2} is equal to one in the model of Bayer and Foster. The momentary soot oxidation temperature $T_{s,ox}$ used in equation (6) is taken equal to the adiabatic flame temperature, computed by the equilibrium solver, of the stoichiometric diffusion flame. A single step reaction from pure fuel to complete combustion products is assumed to compute this temperature.

ADAPTATIONS TO ORIGINAL MODEL – The zero-dimensional approach used by Bayer and Foster results in a computationally efficient model. However, this comes at the cost of some crude approximations. In an attempt to overcome some of these shortcomings, several adaptations are made to the original model.

Fuel mass available – In the original model the fuel mass available for soot formation is given by the balance between the total amount of fuel injected and the cumulative amount of fuel already burnt as derived from the heat release rate. By doing so, the injected amount of fuel present upstream of the initial premixed reaction zone $m_{f,uav}$, see Figure 3, also contributes to the soot formation during the fuel injection period. In reality, this amount of fuel only becomes available at the end of fuel injection. The mass of fuel upstream of the initial reaction zone is therefore subtracted from the momentary fuel injection rate. The corresponding mass of fuel is consumed at the end of injection following a constant rate over the period of time it takes an injected fuel element to reach the initial reaction zone. The available fuel mass is computed from:

$$m_{f,av} = \int_{t_{SOI}}^{t} \dot{m}_{f,inj} dt - m_{f,uav} - \int_{t_{SOC}}^{t} \frac{ROHR_{diff}}{LHV} dt \qquad (7)$$

where *LHV* is the lower heating value of the fuel.

In contrast to Bayer and Foster only the diffusive combustion phase is considered. It is postulated that the fuel that burns as premixed does not lead to significant soot formation. Therefore, only the diffusive part of the heat release rate is used in equation (7). The fuel mass associated with the premixed burn is subtracted from the instantaneous fuel injection rate.

Soot oxidation temperature – In the soot model presented by Bayer and Foster, the soot oxidation temperature changes instantaneously to the mean bulk gas temperature at the end of combustion. In doing so, it is implicitly assumed that soot oxidation continues to occur at the stoichiometric diffusion flame, with corresponding high temperatures, until the end of combustion. In reality, the steady combusting fuel spray, as assumed in the model, gradually breaks up into smaller soot formation clouds before the end of combustion. As a result of this break up, a steady combusting spray is no longer present and soot particles can avoid oxidation at the diffusive reaction layer. These soot particles are (partially) oxidized at lower temperatures and off-stoichiometric conditions. In an attempt to obtain a more realistic description of the oxidation process during the final stages of the combustion process, a more gradual decrease of the oxidation temperature from the adiabatic flame temperature to the bulk gas temperature is used by introducing a mixing time scale τ_{EOSS}:

$$T_{s,ox}(t) = T_{ad,EOSS} - \left(T_{ad,EOSS} - T_{bulk}(t)\right) \cdot \left(1 - e^{\frac{t - t_{EOSS}}{\tau_{EOSS}}}\right) \quad (8)$$

where $T_{ad,EOSS}$ is the adiabatic flame temperature at the assumed End Of Steady-State (EOSS) combustion.

Oxygen dependency – Preliminary simulations, using the original soot model, showed that the model was not able to correctly describe the increase in soot mass for increased EGR rates. To overcome this shortcoming, an additional tuning parameter C_{O_2} is introduced on the molar oxygen concentration in the soot oxidation rate expression, see equation (6). Because the equivalence ratio of the premixed initial reaction is unaffected by the residual gas fraction [15], the source of found deviation is believed to be in the soot oxidation. The soot oxidation process is primarily a particle surface oxidation process. The actual ambient oxygen concentration is therefore likely to have a great influence. By introducing the parameter C_{O_2}, the influence of EGR, which lowers the ambient oxygen concentration, on soot oxidation is increased. A value of 2.5 is found as a best fit.

MODEL VALIDATION

Figure 4 shows an overview of the different chronological steps taken to validate the emission formation model. The result of this process is an emission model for which the modeling concept has been validated, but which is not yet optimized regarding computational effort. This will be the main focus of planned future research to obtain a real-time emission model. The different steps taken during the validation process will be described in more detail in the following sections.

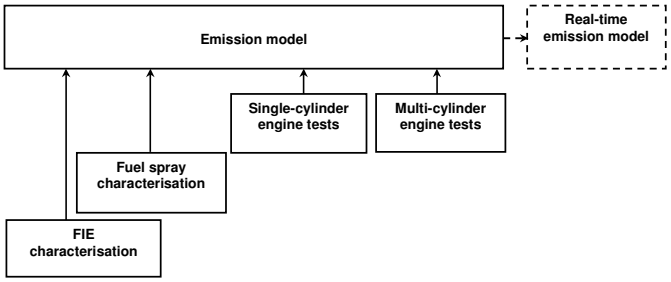

Figure 4 Overview of model validation process

FIE CHARACTERISATION - The first step in the validation process is the characterization of the Fuel Injection Equipment (FIE), which is of the Common Rail type. Both the NO and soot model are very dependent on inputs associated with the fuel injection process: the fuel mass flow rate and fuel exit velocity as is clear from equations (2) and (7) for example. Through the characterization of the FIE equivalent injection profiles, for the injection parameters set during a given engine test, can be reconstructed. The fuel injection rate is reconstructed as a top-hat profile with finite opening and closing times.

For the reconstruction of both the fuel injection rate and corresponding fuel exit velocity, the flow through the injector nozzle needs to be characterized by determining two specific flow coefficients: the discharge coefficient C_d and the velocity coefficient C_v. These coefficients quantify the influence of cavitation on respectively the mass flow rate and fuel exit velocity. At the Combustion Technology group of the Eindhoven University of Technology full characterization of the nozzle flow is achieved by performing both mass flow rate and momentum flow rate measurements using dedicated experimental set-ups. Mass flow rates are measured using the method suggested by Zeuch [16]. More details on these measurements can be found in [17],[18]. The momentum flow rate is directly measured by impinging a fuel spray onto a force sensor. The required coefficients can be determined by combining both types of measurements considering that:

$$\dot{m}_f = A_{noz} \cdot \rho_f \cdot U_f = C_d \cdot A_{noz} \cdot \rho_f \cdot \sqrt{2\Delta p / \rho_f} \quad (9)$$

$$\dot{M}_f = \dot{m}_f \cdot U_f = \dot{m}_f \cdot C_v \cdot \sqrt{2\Delta p / \rho_f} \quad (10)$$

where ρ_f the fuel density, A_{noz} the geometrical nozzle flow area, Δp the pressure differential across the nozzle holes. Frequently, two additional flow coefficients are used. The area contraction coefficient C_a, which is defined as the ratio of the discharge coefficient to the velocity coefficient describes the loss in flow area by cavitation. Subsequently, the product $C_a \cdot C_v^2$ is referred to as the momentum coefficient C_M. Besides for the nozzle flow characterization, the mass flow rate measurements are also used to quantify the dynamics of the fuel injection process regarding the injection timing and the rise and fall rates of the mass flow rate during opening and closing of the injector. This is required to obtain accurate values for the actual start of injection as a function of rail pressure and injector start of actuation.

FUEL SPRAY CHARACTERISATION – The next step in the model validation process is the characterization of the fuel spray. In both the NO formation model and the soot formation model characteristic spray parameters are required: the spray cone angle, spray penetration distance, liquid length and flame lift-off length.

At the Eindhoven University of Technology extensive spray (combustion) analysis is performed in the Eindhoven High Pressure Cell (EHPC) using several optical techniques. Spray penetration and spray cone angle are determined using the Shadowgraphy and Schlieren method. Mie-scattering is used for liquid length determination. Flame lift-off lengths are determined using line of sight laser extinction techniques to measure soot incandescence. For more information regarding these measurements and results please refer to one of the following papers [18], [19],[20].

Measurement data can be used to develop databases with required spray information or existing correlations for spray penetration, cone angle and flame lift-off length can be tuned to the specific FIE.

SINGLE-CYLINDER ENGINE – The emission models are first validated on the basis of measurement data of a research type single-cylinder heavy-duty direct injection diesel engine.

The base engine is a six-cylinder heavy-duty DI diesel engine from which one cylinder is isolated and used for combustion and exhaust gas concentration measurements. Three cylinders are used for motoring of the test-cylinder. Two cylinders are non-firing cylinders that function as EGR pumps. The purpose of these cylinders is to generate adequate EGR pressure even at recirculation levels in excess of 60 wt-% and up to 5 bar charge pressure. The main engine specifications are listed in Table 1.

Table 1 Main specifications of single-cylinder engine

Geometrical engine data	
Base engine	6 -cylinder, HD DI diesel
Cylinders [-]	1 isolated for combustion
Bore [mm]	130
Stroke [mm]	158
Compression ratio [-]	16.0
Piston bowl shape	M-shaped
Diameter piston bowl [mm]	100
Fuel injection system	
Type	Common rail
Max. injection pressure	1300 bar
Number of nozzle holes	8, equally spaced
Nom. hole diameter [mm]	0.178
Cone angle	154°

Test programme – The data set used for model validation consists of several sweeps to analyze the influence of injection timing, engine speed and injection pressure for various EGR rates. The sweeps are performed on two nominal operating points, see Table 2. NO concentrations are measured using a HORIBA MEXA – 7000 analyzer. Soot mass values are derived from Filter Smoke Numbers (FSN) measured with an AVL Smoke meter type 415S. An engine specific correlation has been developed to convert the FSN values to actual soot mass values.

Net heat release rate is derived from measured in-cylinder pressure data by standard first law of thermodynamics analysis [10]. In-cylinder pressure is measured using an AVL GU21C piëzo-electric pressure sensor. The pressure curves are filtered using a Savitsky-Golay smoothing filter. Using this filter leaves combustion efficiency unchanged, the Start Of Combustion (SOC) is however advanced by about 0.7 ca. Blow-by is neglected and heat loss is computed using the well-known Woschni-correlation [21]. The constants in this correlation are scaled such that gross cumulative heat release matches the amount of fuel injected.

Table 2 Measurement matrix for single-cylinder engine

Variable	**Point 1**	**Point 2**
Engine speed [rpm]	1500	1500
IMEP [bar]	14.0	7.0
Lambda (0% EGR)	1.8	3.2
Injection pressure [bar]	900	750
Actuation duration [ms]	3.5	2.1

Sweep	**Var. [°ca aTDC] / [rpm]/ [bar]**	**EGR m-%**	**Ref.**
A, B,C	SOA -30:5:+0	0,25,50	2
D,E,F	SOA -20:5:+5	0,15,30	1
G,H,I	N_{eng} 1000 1500 2000	0,25,50	2
J	p_{inj} 500 750 1000	25	2
K	p_{inj} 500 1000 1300	0	1; N_{eng} = 1000

FIE characterization – The fuel injection equipment of the single-cylinder engine, see Table 1 for specifications, is characterized by performing single-shot mass flux and momentum flux measurements as described earlier. Figure 5 gives an overview of the derived flow coefficients as a function of cavitation number. The vertical line in Figure 5 indicates the transition to a non-cavitating flow. Here, the effective discharge coefficient is no longer a function of the cavitation number. However, for normal engine operation, the flow can be assumed to be cavitating and Figure 5 suffices to fully characterize the nozzle flow.

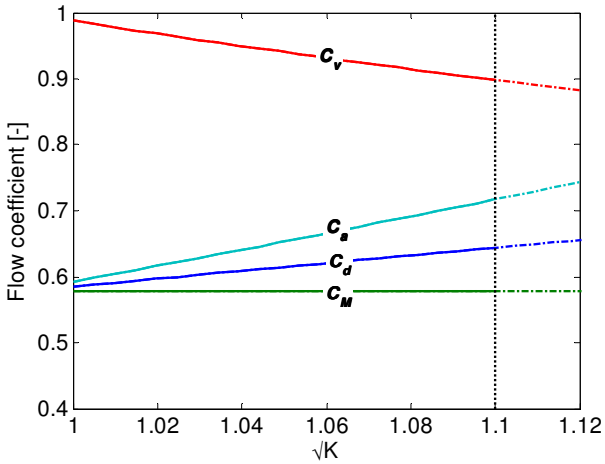

Figure 5 Flow coefficients as function of cavitation number K for nozzle used in single-cylinder engine tests (see Table 1 for specifications).

With use of the data from Figure 5, the fuel injection rate and corresponding fuel velocity corresponding to a certain engine test are reconstructed and used as an input to the NO and soot formation model.

Fuel spray characterization – Required spray information is obtained from correlations found in literature. For the one-dimensional spray model as given by equation (1), Naber et al. and Siebers also developed correlations for respectively the spray penetration [8] and spray cone angle [9]. The area contraction coefficient C_a, determined from the injection measurements, is required

in these correlations. The spray cone angle correlation is tuned such that the moment of spray-wall impingement matches the decrease in the heat release rate profile as a result of impingement. Found cone angles range between 25° – 30°. These values agree well with measured cone angles on similar nozzles in the EHPC [18],[19]. The tuning parameters in the flame lift-off length correlation are determined such that predicted values for the equivalence ratio of the initial rich reaction zone match aforementioned literature values.

MULTI-CYLINDER ENGINE – The validated emission models resulting from the single-cylinder engine tests have also been compared with data from a 6 in-line cylinder heavy-duty DI diesel engine for both conventional and high-EGR combustion [22]. Main engine specifications are listed in Table 3.

Table 3 Main specifications of multi-cylinder engine

Geometrical engine data	
Engine type	HD DI diesel
Cylinders [-]	6
Bore [mm]	130
Stroke [mm]	162
Fuel injection system	
Type	Electronically controlled
Number of nozzle holes	7
Nom. hole diameter [mm]	0.210

Test programme – The operating conditions, listed in Table 4, contain four different 0 wt-% EGR load cases and two injection timings sweeps at 40 wt-% EGR. For all cases the injection pressure is set at 950 bar. All cylinders are equipped with a Kistler piëzo-electric in-cylinder pressure sensor for combustion analysis. Exhaust gas NO emission concentrations are measured for the total engine. Total soot mass is again derived from FSN values using an engine specific correlation. For the high-EGR cases a specially designed correlation is used. Pressure signal handling and heat release rate computation procedure is identical as for the single-cylinder engine or as mentioned when otherwise.

Table 4 Operating conditions for multi-cylinder tests

Variable	**1**	**2**	**3**	**4**	**L**	**M**
Speed [rpm]	1600	1200	1830	1830	1830	1200
IMEP [bar]	7.6	8.5	13.1	5.7	5.8	6.8
Lambda	2.3	2.6	2.2	3.1	~1.7	~1.5
Actuation dur. [ms]	1.4	1.1	2.4	1.0	Varied*	Varied*
EGR-%	0	0	0	0	40	40
SOA [°ca aTDC]	-10	-10	-10	-10	Varied	Varied

* Varied for maintaining fixed IMEP

For the multi-cylinder engine manifold conditions are not measured for each individual cylinder, i.e. close to the respective intake port. Determination of the initial in-cylinder conditions are based on the same measured manifold conditions measured in between cylinders 3 and 4. No corrections are made to take into account deviations between the different cylinders.

FIE and spray characterization – In contrast to the FIE of the single-cylinder engine, the fuel injection system of the multi-cylinder engine has not been characterized. This means that no exact values are present for the actual Start Of Injection (SOI). Fuel injection rates are reconstructed on the basis of the injection measurements performed on the FIE for the single-cylinder engine. The required discharge coefficient is derived from measured injected mass flow rates on the engine. The remaining flow coefficients are scaled on the basis of the coefficients found for the nozzle used in the single cylinder engine tests.

Fuel spray characterization for the FIE of the multi-cylinder engine is performed analogous to the procedure used for the single-cylinder engine.

SENSITIVITY ANALYSIS

It is well-known that NO formation is extremely temperature sensitive. As a result, accurate determination of the initial in-cylinder conditions at Intake Valve Closing (IVC) is of great importance. In this study, in-cylinder charge is assumed to be an ideal gas. The initial in-cylinder temperature at IVC is determined using the semi-empirical correlation suggested by Zapf [23] for 4-stroke diesel engines. Since in-cylinder volume is known from the crank-slider kinetics, in-cylinder mass is defined when the in-cylinder pressure at IVC is known. The in-cylinder pressure curves are pegged such that the cumulative mass flow rate through the intake valves (calculated using the compressible valve-flow equation [10]), matches the measured inducted mass. Inducted mass flow rates are measured using a MICRO MOTION coriolis-type mass flow meter. As a result of the intermittent gas exchange process, mass flow rates and manifold pressures are unsteady. For the single-cylinder engine, the influence of the resulting uncertainty in inducted measured mass on the in-cylinder pegging procedure and final NO formation has been analyzed.

Figure 6 gives an shows how the uncertainty in measured inducted mass influences the accuracy of the initial combustion product temperature prediction and subsequently predicted NO emission index for the three EGR cases (Operating details given in Table 2, sweeps A, B and C for SOA = -15 °ca aTDC). The EINO result for the 50% EGR case is repeated on a different scale for clarity. In the used engine set-up the uncertainty in measured inducted mass increases slightly with applied EGR rate as a result of more severe oscillations in measured mass flow rate.

Although relative deviations in measured mass flow rate and predicted temperature are very small, the high temperature sensitivity of NO formation causes the relative error on the predicted NO emission index to be high. NO prediction with accuracy levels below 10% are

difficult to obtain. This has to be considered when using NO models on-line as virtual NO sensors [3].

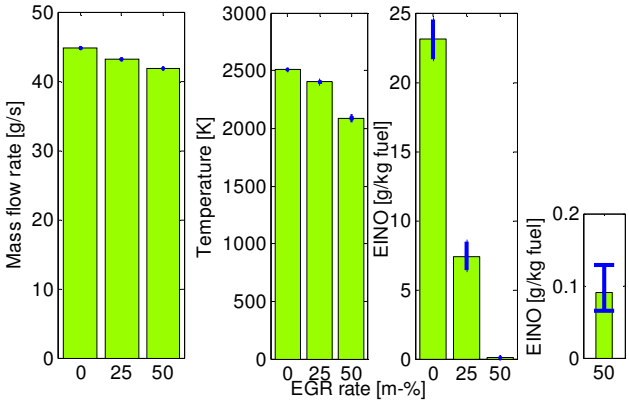

Figure 6 Influence of uncertainty on measured mass flow rate on NO emission for SOA = -15 °ca aTDC point of sweeps A, B and C (7 bar IMEP at 1500 rpm), see Table 2 for operating conditions.

RESULTS

Results will be presented for the single-cylinder engine and subsequently for the multi-cylinder engine. For both engines, first NO emission predictions will be compared with measurements followed by the soot prediction results. For the single-cylinder engine also the importance of the different phenomena determining the (initial) combustion products temperature for NO reduction will be presented. For the multi-cylinder engine the differences in emission formation between the individual cylinders is analyzed in order to determine whether it suffices to predict total engine-out emissions on the basis of a measured in-cylinder pressure curve of just one cylinder.

SINGLE CYLINDER ENGINE

NO emission

Injection timing variation – Injection timing influences ignition delay and the amount of fuel that burns during the premixed combustion phase. Higher premixed burn rates results in higher pressure rise early in the combustion cycle. The corresponding temperature increase results in higher NO formation rates. As mentioned earlier, NO formation from fuel burnt as premixed is assumed to be negligible and only the diffusive combustion phase is considered. To validate this assumption, the Start Of Actuation (SOA) has been varied for both nominal operating points and various EGR rates. Figure 8 shows the results of SOA sweeps on nominal operating point 1 for three different EGR levels, see Table 2 for specifications. For the 0% EGR cases, the corresponding main inputs are shown in Figure 7 as reference. The diffusion combustion is assumed to occur when the premix burn rate peaks. For the calculations, the initial start of the diffusion burn is fitted with a Wiebe function. The used heat release rates are given by the solid lines in Figure 7.

Figure 8 shows that for the applied SOA, good qualitative agreement is present. Predicted NO emission indices (EINO) are within 25% of measured values. This level of accuracy is not sufficient for the model to be used as on-line virtual NO sensor, but is comparable with, if not better than, current state-of-the-art NO models for controller development.

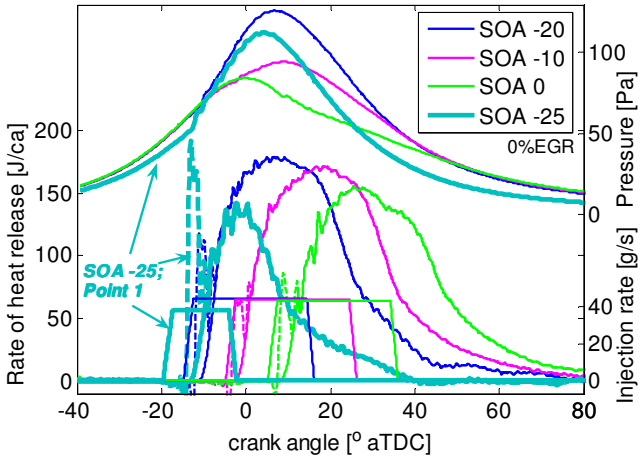

Figure 7 In-cylinder pressure, Gross rate of heat release and fuel mass injection rate for three Start Of Actuation timings of sweep D (1500 rpm, IMEP 14.0 bar) and SOA – 25 °ca aTDC case of sweep A (1500 rpm, IMEP 7.0 bar), see also Table 2.

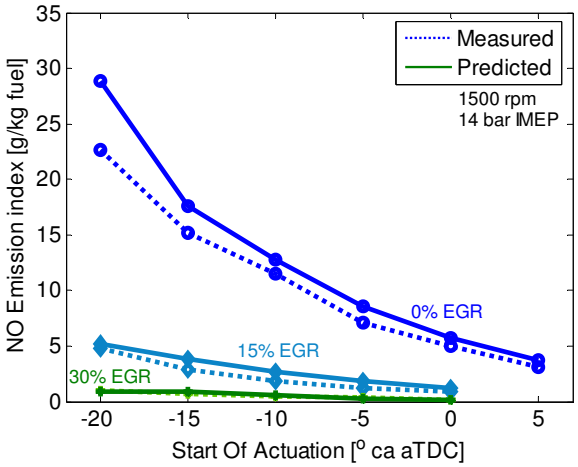

Figure 8 Measured and predicted NO emission index for sweeps D, E and F as listed in Table 2.

Figure 9 shows the results for the SOA sweeps on nominal operating point 2 for three different EGR levels, see Table 2 for specifications. In Figure 7 the corresponding inputs for the case of SOA = -25 °ca aTDC and 0% EGR is also shown. Figure 9, shows that for early injection timings (SOA before -15 o ca aTDC), predicted NO emissions are too low. It is found that the deviation becomes more pronounced when premixed burn rates are higher. As can be observed in Figure 7, the premixed burn rates for the SOA = -25 °ca aTDC case is much higher than for the other depicted cases. This indicates that for advanced injection timings (SOA before -15 °ca aTDC), the contribution of the premixed burnt fuel to NO formation cannot be simply neglected. It

is believed that the increase in local temperature corresponding to the high premix burn rates is not well captured by the model. Also, for the fuel-rich premixed burn phase, other NO forming mechanisms than accounted for in the model, could be of importance, e.g. prompt NO.

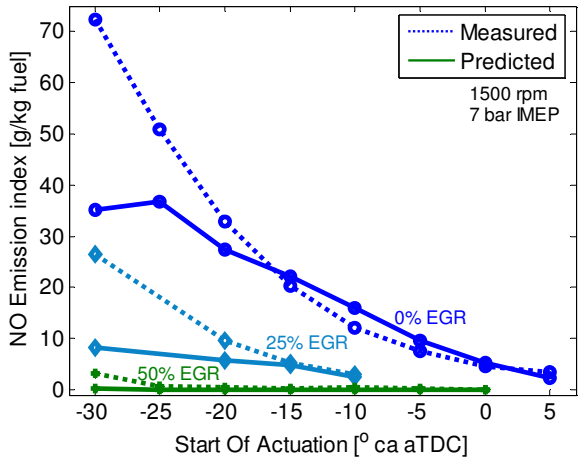

Figure 9 Measured and predicted NO emission index for sweeps A, B and C as listed in Table 2.

Engine speed variation – The time available for the NO kinetics to form NO is proportional to the engine speed. Variation of the engine speed is used to verify the used NO formation mechanisms. In Figure 10, the results are shown for a variation in engine speed at three different EGR rates. Start of actuation is held fixed at -15 °ca aTDC. The results indicate that the dominant NO formation kinetics are correctly taken into account.

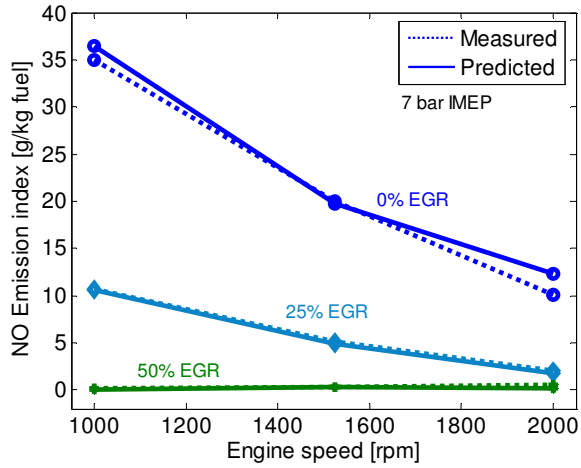

Figure 10 Measured and predicted NO emission index for sweeps G, H and I. as listed in Table 2.

Injection pressure variation – As mentioned before, the fuel spray is the primary energy source for the mixing process. Oxidizer entrainment into the combustion product packages is therefore based on a model of the fuel spray. The turbulent kinetic energy in the fuel spray is determined by the fuel injection pressure. The injection pressure is varied as a check on the used approach for combustion product package dilution. The influence of fuel injection pressure on the NO emission index is shown in Figure 11. Increasing the fuel injection pressure, results in a higher amount of fuel that becomes available for combustion during the ignition delay period. This leads to higher premix burn rates and corresponding higher temperatures in the early stages of combustion. The result is an increased NO emission formation rate. Shorter residence times as a result of the higher mixing rates only partly counteract this NO formation increase. The general trend of increased NO with higher injection pressure is captured quite well by the model. However, for the case of 500 bar injection pressure, the model consequently overestimates the NO formation. Injection duration is the longest for this case (to keep IMEP constant). As a result of the longer injection duration, spray penetration is larger and the spray impinges on the piston bowl wall more severely than for the other operating points. Spray-wall impingement changes the mixing rates and the assumed mixing model, which is based on a model of a free spray, needs adaptation. This will be part of future research.

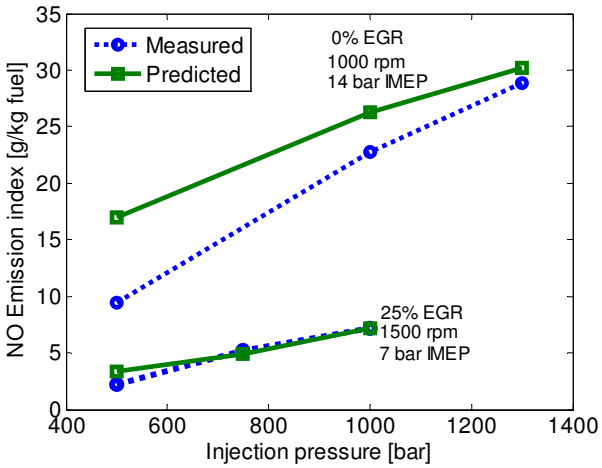

Figure 11 Measured and predicted NO emission index for sweeps J and K as listed in Table 2.

Effect of flame temperature correction on NO formation – The initial combustion product temperature is based on the adiabatic flame temperature. This temperature is corrected for: evaporative cooling, soot radiative cooling, turbulence effects (i.e. flame strain) and gas radiation. Figure 15 presents an overview of the fraction of total predicted NO emission associated to a specific temperature correction phenomenon for sweeps A, C, D and F (see Table 2). In the figure also the absolute value of the decrease in EINO and the final NO emission index are shown. The temperature reducing phenomena result in a decrease in NO emission up to a factor of two. This shows the importance of including flame cooling phenomena. General trends are found to be the same for all cases. Flame temperature reduction by flame strain, i.e. turbulence, is found to be the primary NO reducing mechanism for all considered cases. Soot radiation is also significant and increases in importance when injection timing is advanced due to higher soot production. The decrease of NO formation as a result of evaporative cooling is also of importance and remains fairly constant when changing injection timing. Gas radiation has only a minor influence with a corresponding

NO decrease of about 3% for all considered cases. It can be neglected to decrease model complexity and computational effort without significant loss in accuracy.

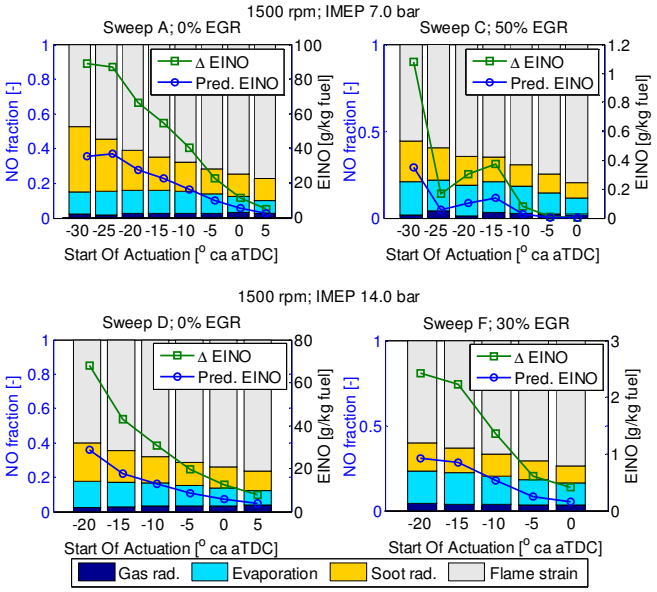

Figure 12 Contribution of different temperature NO reducing phenomena to NO emission index change (ΔEINO) together with the corresponding final predicted NO emission index. See Table 2 for operating conditions.

Soot emission - During the combustion process high amounts of soot can be present inside the combustion chamber. However, most of this soot is oxidized before it can enter the exhaust system. Because the net soot production is the balance of two high rates, as indicated by equation (4), accurate quantitative soot mass prediction is very difficult. The soot formation model therefore focuses on qualitative agreement rather than high quantitative accuracy.

Injection timing variation – Injection timing determines the amount of fuel that burns as premixed and has great influence on combustion temperature. One of the adaptations made to the original soot model of Bayer and Foster is the postulation of no soot formation from the premixed burnt fuel. Varying the injection timing is used to verify this postulation. Figure 13 presents the results for three different SOA sweeps at three EGR levels. The results show a gradual increase in soot mass as injection timing is retarded. As injection timing is retarded, the centroid of combustion shifts more into the expansion stroke where temperatures are lower and less time is available for soot oxidation. This general trend is captured very well by the model as indicated by the coefficients of determination, i.e. R^2 values.

For the highest EGR case and injection timings retarded beyond -10 °ca aTDC, temperatures are low enough to limit the soot formation rate such as to decrease the net soot production. This decrease in formation rate is not correctly captured by the model as is shown in Figure 13. Although the soot production levels off, soot formation remains too high for these retarded injection timings. This deviation is not contributed to the omission of soot formation from the premixed burn fuel. The good qualitative agreement as given by R-square values indicated in Figure 13, also suggests that the postulation of no soot formation resulting from the premixed burn phase is correct or at least does not give rise to significant errors.

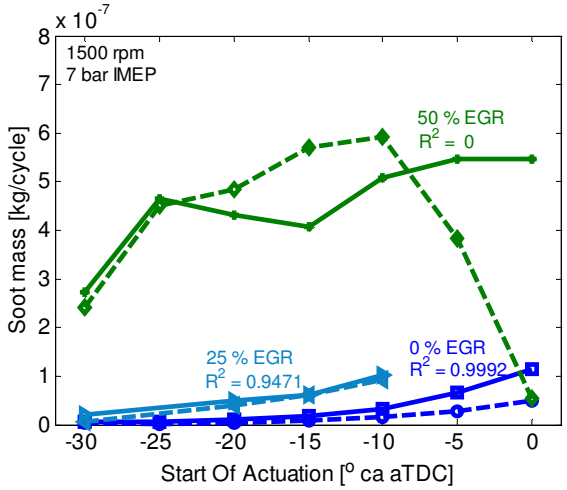

Figure 13 Measured and predicted soot emission for sweeps A, B and C as listed in Table 2 . R^2 values are determined after normalizing the data on the most retarded injection timing.

Engine speed variation – The variation in engine speed is used to analyze the influence of the time available for soot production. As engine speed is increased, there is more time available for soot oxidation which reduces the net soot mass produced. Figure 14 shows that this trend is correctly described by the model.

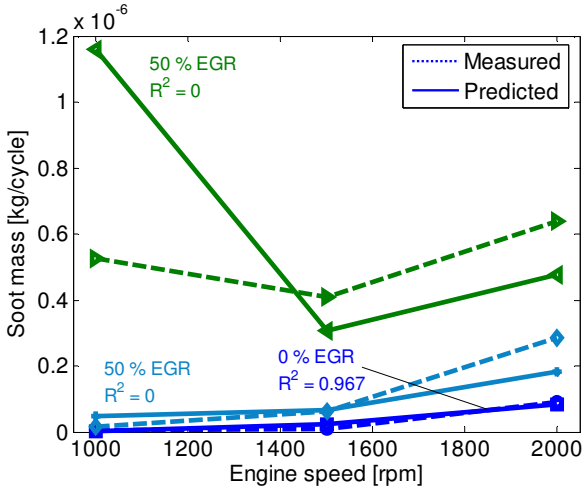

Figure 14 Measured and predicted soot emission for sweeps G, H and I. as listed in Table 2. R^2 values are determined after normalizing the data on the highest engine speed.

Injection pressure variation – The flame lift-off length is dependent on the fuel injection pressure. Higher injection pressures increase the lift-off length and allows more oxidizer to be entrained upstream of the premixed initial reaction zone. This reduces the equivalence ratio of the initial premixed reaction zone, resulting in a lower soot

formation rate. This trend can be seen in both the measured and predicted soot mass as can be seen in Figure 15. As for the NO emission model, the results for the lowest injection pressure cases differ the most. Here again the effect of spray-wall impingement is believed to be the main cause. Fuel that hits the wall (partially) avoids the oxidation process. The measured heat release rate decreases as a result of this. Following from equation (7) the soot formation rate will increase as a result of more available fuel mass. The predicted increase is however not sufficient to capture the observed increase in net soot production. More physics have to be included to fully quantify the effect of spray-wall impingement.

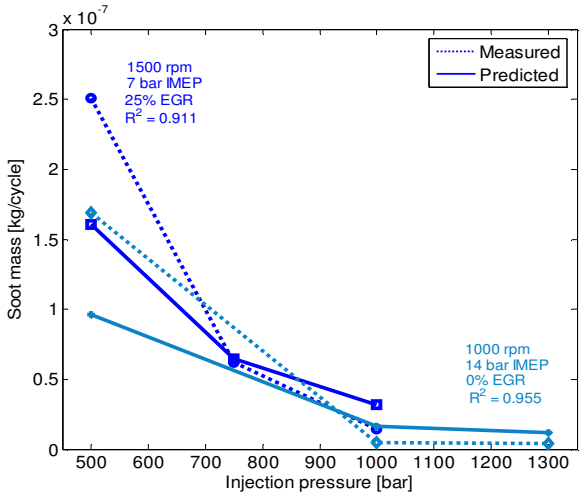

Figure 15 Measured and predicted soot emission for sweeps J and K as listed in Table 2. R^2 values are determined after normalizing the data on the highest injection pressure.

EGR-rate variation – As mentioned before, an additional tuning parameter on the soot oxidation rate had to be introduced to obtain acceptable quantitative agreement for increased EGR levels. From the presented results described above, it can be concluded that the use of this parameter gives satisfying results for considered changes in operating conditions at the different EGR levels. Providing a more physical basis to capture the influence of EGR on soot production will be part of future work. In general, it can be concluded that there is a good qualitative and even acceptable quantitative agreement for early and advanced injection timings over a broad range of operating conditions.

MULTI-CYLINDER ENGINE - NO and soot formation is computed using the actual heat release rate of each cylinder. Due to absence of individual cylinder fueling and gas exchange data, fueling and gas exchange of each cylinder are taken identical.

Compared to the model of the single-cylinder engine, only the engine specific model parameters related to the fuel injection system and combustion chamber geometry have been changed. If the models are indeed generic, this will not result in a loss in accuracy. The accuracy of predicted NO and soot emission will be shown first. Thereafter analysis will focus on observed differences in emission formation between the individual cylinders.

Total engine averaged emissions

NO emission – The measurement matrix for the multi-cylinder engine contains four different load and engine speed cases at 0 % EGR, spread over a significant part of the engine operating range, see Table 4. The measured and predicted NO formation indices for these load cases are shown in Table 5. The deviations between predicted and measured EINO indicated in the table are of the same order as found for the single-cylinder engine. Since the model parameters are the same as for the single-cylinder engine, this shows that, at least for used range of operating conditions and engines, the model is indeed generic.

Table 5 Measured and predicted NO emission index for the 0 % EGR operating conditions as listed in Table 4.

Operating point	Meas. EINO [g/kg fuel]	Pred. EINO [g/kg fuel]	Deviation
1	51.7	62.0	+19.9%
2	25.9	30.8	+18.9%
3	19.5	24.3	+24.6%
4	22.7	31.5	+38.8%

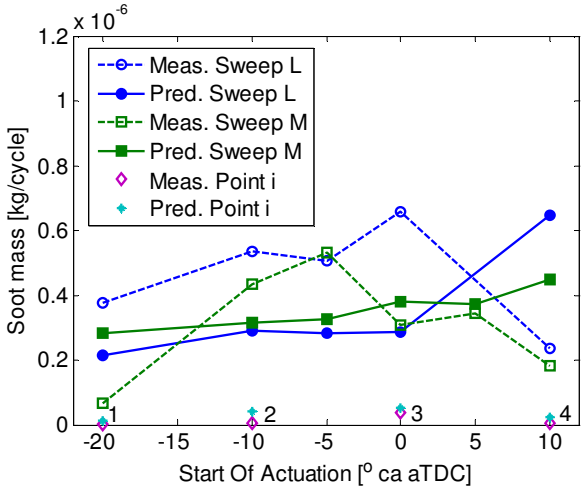

Figure 16 Measured and predicted soot mass for two SOA sweeps at 40% EGR and 0% EGR load cases as listed in Table 4.

Soot emission – Figure 16 gives an overview of the predicted and measured soot emission for all operating points listed in Table 4. It has to be noted that the x-axis only applies to the two 40% EGR cases. For the 0% EGR operating points SOA = -10 °ca aTDC. Soot emission for the 0% EGR cases is virtually zero, which is correctly predicted by the model. The measured soot emissions for the two high-EGR SOA sweeps listed in Table 4, show the same trend as found for the single-cylinder engine: at retarded injection timings, the soot formation rate decreases and net soot production drops. The soot model is again not able to capture this phenomenon. For conventional timings (between SOA = -15 and 0 °ca aTDC), the agreement between predicted and measured soot levels is reasonable. Here, it can

however be expected that more detailed information on actual fueling rates results in improved agreement.

Individual cylinder emissions – Previous predicted emissions are average values of predicted results for each individual cylinder. The differences in predicted NO and soot emission between the individual cylinders has been analyzed to answer the question whether total engine out emissions can be predicted with acceptable accuracy on the basis of only one cylinder pressure curve. If so, this limits the need to equip each cylinder with a pressure sensor reducing system complexity, costs and computational effort.

NO emission – Figure 17 shows the measured total NO emission index and the predicted EINO for each individual cylinder for an SOA sweep at 40% EGR rate (Sweep L, see Table 4). All cylinders globally show the same trend but absolute levels differ by max. ± 25 %. The relative deviation between the different cylinders becomes smaller when injection timing is retarded. Corresponding flame temperatures are reduced to levels where NO formation through the Zeldovich mechanism is less dominant. The temperature sensitivity of NO formation is therefore reduced for retarded injection timings and differences in temperature become less pronounced in predicted EINO values.

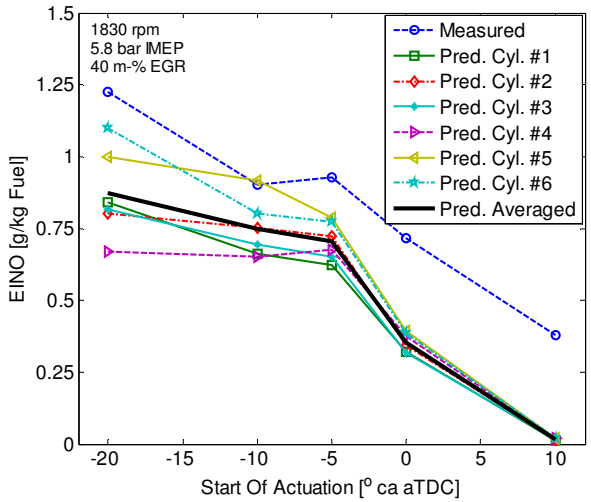

Figure 17 Measured and predicted NO emission index for Sweep L (see Table 4) for the six individual cylinders.

Soot emission – Soot emissions have also been computed for each individual cylinder on the basis of the corresponding heat release rate profile and reconstructed fuel injection profile. Figure 18 shows the results for operating condition 4 as listed in Table 4. Although the averaged soot mass is in good agreement with the measured values, deviations between the different cylinders are relatively large with a standard deviation of ± 15% of the average value.

The results for both the NO and soot emissions show that data from all individual cylinders is required to obtain the best agreement with measured total engine-out emission values.

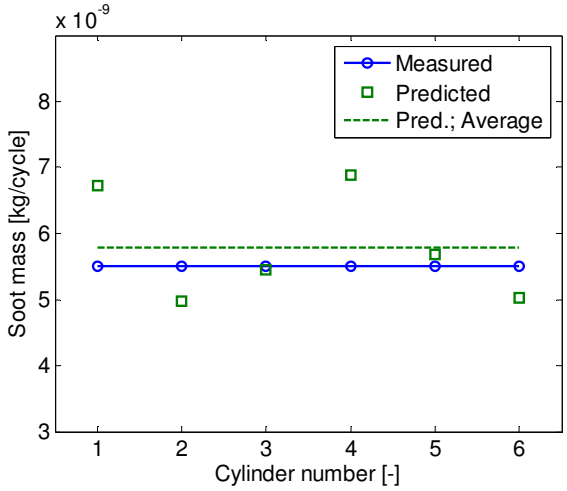

Figure 18 Measured total soot mass and predicted soot mass for individual cylinders for operating point 4 as listed in Table 4.

COMBINED RESULTS - Figure 19 and Figure 20 give an overview of the modeling accuracy comparing all measured and predicted NO respectively soot emissions for both the single-cylinder and the multi-cylinder engine.

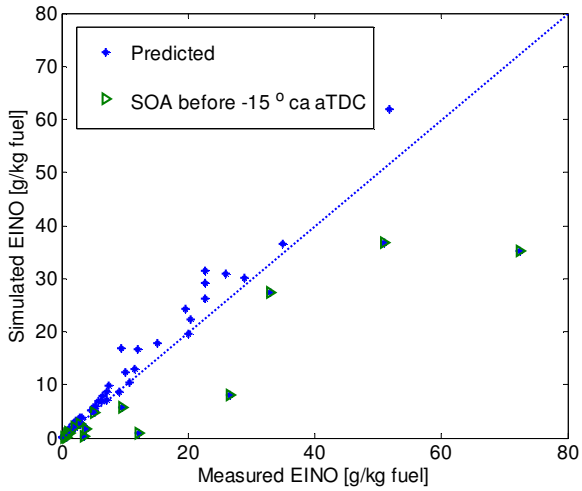

Figure 19 Overview of measured and predicted NO emission index.

For the NO formation model the agreement is very good when excluding the operating points with injection timing before -15 °ca aTDC. An R^2 of 0.92 is obtained. Including these operating points results in an R^2 of 0.81.

Figure 20 represents an overview of the soot model results. Table 6 gives an overview of the coefficients of determination. The R-square values including the multi-cylinder data are significantly lower. This is contributed to the fact that predicted results are not based on cylinder specific data regarding the gas exchange process to determine the initial in-cylinder conditions and fueling rates. Increasing the accuracy will come at the cost of additional sensors. As mentioned before, the soot model is not capable of predicting the decrease in net soot production for late DI operating points (SOA beyond TDC). Excluding the late DI operating points significantly

improves the coefficients of determination for both the single-cylinder and the multi-cylinder engine data as is indicated in Table 6.

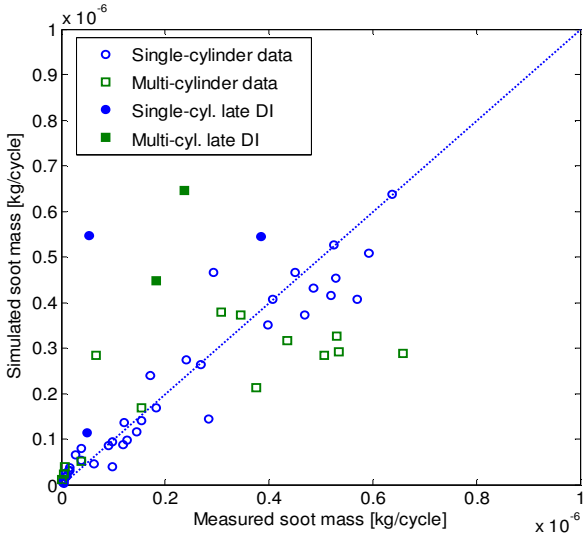

Figure 20 Overview of measured and predicted soot mass.

Table 6 Overview of R^2 values for the soot model

Single + Multi cylinder		
SOA timings R^2	Incl. late DI 0.547	Excl. late DI 0.736
Single-cylinder		
SOA timings R^2	Incl. late DI 0.695	Excl. late DI 0.839

CONCLUSION

The experimental validation process of an extended phenomenological NO model and a newly added state-of-the-art soot model are described. Predicted NO and soot mass emissions show good qualitative agreement with measured values for conventional DI diesel combustion and high-EGR combustion (up to 50% EGR) with conventional injection timing. NO predictions are generally within 20% of measured values for aforementioned combustion concepts. This level of accuracy is in-line with comparable state-of-the-art emission models found in literature which commonly have a more (semi-)empirical nature. Only the increase in soot formation for increasing EGR rates had to be corrected for by introducing a semi-empirical tuning parameter. Predicted results for both a single-cylinder and multi-cylinder engine show acceptable accuracy with the same set of model parameters (excluding geometrical engine parameters). This indicates that the developed models are generic for the considered engines and operating ranges.

Predicted soot and NO emission between the individual cylinders of a multi-cylinder engine showed deviations in the order of respectively ±15% and ±25% of the total engine-out emissions. Part of the observed deviations can be contributed to the fact that no deviation in individual fueling rate and gas exchange conditions for the different cylinders could be made. Improving accuracy will come at the cost of additional sensors which may not be desired.

The high temperature sensitivity of NO formation, results in a high sensitivity of predicted NO emissions to set initial conditions at Intake Valve Closing. In-cylinder pressure curve pegging is performed on the basis of measured inducted mass flow rates. Simulation results show that obtaining NO emission accuracy within ±10% is very difficult even with non-automotive mass flow meters.

Flame temperature decrease by flame-straining as a result of turbulence is found to be a primary NO reducing factor. Radiative cooling by soot radiation and evaporative cooling also contribute significantly to NO formation reduction. The influence of gas radiation is negligible and can be omitted to increase computational efficiency without negatively influencing model accuracy.

Future work will include the implementation of developed emission model into TNO's current DYNAmic Engine MOdel DYNAMO. This requires optimizing the model regarding computational effort such that the model can also be used as a combustion state estimator in a real-time environment. Next, model development will concentrate on extending the models to other advanced combustion concepts, e.g. HCCI.

ACKNOWLEDGMENTS

The authors would like to thank TNO automotive for financial support and multi-cylinder engine data.

REFERENCES

1. Timoney, D.J., Desantes, J.M., Hernandez, I., Lyons, C.M. (2005), The development of a semi-empircal model for rapid NOx concentration evaluation using measured in-cylinder pressures in diesel engines, Proc. IMechE, Jl. Aut. Engng., Vol. 129, Part D
2. Andersson, M., Johansson, B., Hultqvist, A., Nöhre, A., A real time NOx model for conventional and partially premixed diesel combustion, SAE paper 2006-01-0195, 2006
3. Arrègle, J., Javier López, J., Guardiola, C., Monin, C., Sensitivity study of a NOx estimation model for on-board applications, SAE paper 2008-01-0640, 2008
4. Baert, R.S.G., Seykens, X.L.J., Phenomenological NO model for conventional heavy-duty diesel engine combustion, in Internal Combustion engines: Performance, Fuel Economy and Emissions, IMechE, London, United Kingdom, 2007
5. Murayama, T., Miyamoto, N., Sasaki, S., Kojima, N., The relation between nitric oxide formation and combustion process in diesel engines, Proc. 12th Int. Congr. On Combustion Engines, Vol. B, CIMAC, Tokyo, 1977

6. Dec, J.E., Canaan, R.E., PLIF imaging of NO formation in a DI diesel engine, SAE paper 980147, 1998
7. Verbiezen, K., Donkerbroek, A.J., Klein-Douwel, R.J.H., van Vliet, A.P., Frijters, P.J.M., Seykens, X.L.J., Baert, R.S.G., Meerts, W.L., Dam, N.J., ter Meulen, J.J. (2007), Diesel combustion: In-cylinder NO concentrations in relation to injection timing, Combustion and Flame, Vol. 151
8. Naber, J.D., Siebers, D.L., Effects of gas density and vaporization on penetration and dispersion of diesel sprays, SAE paper 960034, 1996
9. Siebers, D.L., Scaling liquid-phase fuel penetration in diesel sprays based on mixing-limited vaporization, SAE paper 1999-01-0528
10. Heywood, J.B. Internal Combustion Engines Fundamentals, McGraw-Hill, London, 1988, ISBN 0-07-028638-8.
11. Bayer, J., Foster, D.E. Zero-dimensional soot modeling, SAE paper 2003-01-1070, 2003
12. Dec, J.E., A conceptual model of DI diesel combustion based on laser-sheet imaging, SAE paper 970873, 1997
13. Hiroyasu, H., Kadota, T., Development and use of a spray combustion modeling to predict diesel engine efficiency and pollutant emissions – Part I Combustion modeling, Bulletin of the JSME, Vol. 26, No. 214, 1983
14. Chomiak, J., Karlsson, A., Flame liftoff in diesel sprays, 26th International Symposium on Combustion, 1996
15. Siebers, D., Higgins, B., Flame lift-off on direct injection diesel sprays under quiescent conditions, SAE paper 2001-01-0530, 2001
16. Zeuch, W., Neue Verfahren zur Messung des Einspritzgesetzes und der Einspritzregelmäßigkeit von Diesel-einspritzpumpen, MTZ No. 9, p 344-349, 1961
17. Seykens, X.L.J., Somers, L.M.T., Baert, R.G.S. (2005), Detailed Modeling of Common Rail Fuel Injection Process, Journal of Middle European Construction and Design of Cars (MECCA), No. 2+3
18. Klein-Douwel, R.J.H., Frijters, P.J.M., Seykens, X.L.J., Somers, L.M.T., Baert, R.S.G. (2008), Gas density and rail pressure effects on diesel spray growth from a heavy-duty common rail injector, Submitted to Energy & Fuels
19. Klein-Douwel, R.J.H., Frijters, P.J.M., Somers, L.M.T., de Boer, W.A., Baert, R.S.G. (2007), Macroscopic diesel fuel spray shadowgraphy using high speed digital imaging in a high pressure cell, Fuel, Vol. 86 (12-13)
20. Frijters, P.J.M., Vallen, R.G.M., Somers, L.M.T., Luijten, C.C.M., Baert, R.S.G., Fuel effects on first soot appearance and soot lift-off length in diesel combustion, Proceedings of the European Combustion Meeting 2007, 2007
21. Woschni, G., A universally applicable equation for the instantaneous heat transfer coefficient in the internal combustion engine, SAE paper 670931, 1967
22. Van Aken, M., Willems, F.P.T., de Jong, D., Appliance of high EGR rates with short and long route EGR system on a Heavy Duty diesel engine, SAE paper 2007-01-0906, 2007
23. Zapf, H., Untersuchungen zur Vorausberechnung der Ladungsendtemperatur in Viertakt-Dieselmotoren, MTZ No 31, 1970

NOMENCLATURE

A	Area [m^2]
AFR_{st}	Stoichiometric air-to-fuel ratio [-]
C	Coefficient [-]
d	Diameter [m], discharge [-]
E	Activation energy [J/mol]
K	Cavitation number [-]
LHV	Lower heating value [J/kg]
LL	Liquid Length [m]
LOL	Flame Lift-off Length [m]
m	mass [kg]
$\dot{M}_f$	Fuel momentum flux [N]
p	Pressure [Pa]
R	Universal gas constant [J/Kmol]
$ROHR$	Rate of heat release [J/s]
T	Temperature [K]
t	time [s]
U_f	Fuel velocity [m/s]
x	Axial position [m]
Z_{st}	Stoichiometric mixture fraction [-]
ϕ	Equivalence ratio [-]
ρ	Density [kg/m^3]
θ_{spray}	Spray cone angle [degree]
ad	adiabatic
av	available
$bulk$	bulk
$EOSS$	End of steady-state
f	fuel, formation
inj	injected
noz	fuel injector nozzle
ox	oxidizer, oxidation
s	soot
uav	unavailable
v	velocity

CONTACT

For more information please contact:

Eindhoven University of Technology – Department of Mechanical Engineering – Mr. Xander Seykens
P.O. Box 513 / 5600 MB Eindhoven / The Netherlands
Phone: +31 40 247 5995 / Fax: +31 40 243 3445
E-mail: x.l.j.seykens@tue.nl